Ultralight Graphene

A Versatile, Ultralight, Nitrogen-Doped Graphene Framework**

*Yang Zhao, Chuangang Hu, Yue Hu, Huhu Cheng, Gaoquan Shi, and Liangti Qu**

Herein, we demonstrate a versatile, ultralight, nitrogen (N) doped, three-dimensional (3D) graphene framework (GF). Ultralight materials (less than 10 mg cm^{-3}) have a wide range of applications.[1] Graphene, a 2D single-layer sheet of sp^2-hybridized conjugated carbon atoms, has emerged as a new candidate for construction of low-density materials because of its excellent electrical conductivity, high surface area, good chemical, environmental and mechanical stability, coupled with easy stacking of the layers allowing the formation of 3D structures.[2,3] Graphene-assembled architectures, such as foam and aerogel[2,4] have a tunable hierarchical morphology with high surface areas and can form macroscopic, large-size monolithic materials. These properties has provided a new platform characterized by light weight, high porosity, mechanical stability, and electrical conductivity, thus offering great technological promise for a variety of sustainable applications, such as energy storage, adsorption, and catalysis.[2,4a,5] To date, graphene assemblies have reached a low density of around 5 mg cm^{-3},[4d] but are not yet comparable with the ultralight metallic microlattices (0.9 mg cm^{-3}),[6] and graphitic carbon microtube materials (under 0.2 mg cm^{-3}).[7]

Apart from the geometrical control over the graphene assembly, the other efficient means to functionalize and tune the properties of assembled graphenes is by the regulation of the carbon–carbon bonds within the planar graphene structures. Recent achievements have demonstrated that doping graphene with substituent heteroatoms could effectively modulate the electronic characteristics, surface and local chemical features of graphenes, essential for novel device applications.[8] In this regard, we have developed chemical vapor deposition and electrochemical strategies to create N-doped graphene sheets and dots with unique properties.[9]

Herein, we develop a versatile, N-doped, ultralight 3D GF. The GF is fire-resistant and has an ultra-low density of 2.1 ± 0.3 mg cm^{-3}, which is the lowest that has be achieved to date for a GF architecture (Supporting Information, Table S1). More importantly, the GF exhibits a very high capacity for the reversible adsorption of oils and organic solvents and can be recycled many times. Its adsorption capacity of 200–600 times the weight of the pristine GF sets a record among carbon-based adsorbent materials (Table S2).[4a,e,10] Directly utilized as the active electrode material without any modification, GF has generated a significantly high capacitance of 484 F g^{-1}, approaching to the theoretical electric double-layer (EDL) capacitance of graphene, and far superior to the typical carbonaceous capacitors (Table S3). Further, a new 3D metal-free catalyst of GF for efficient oxygen reduction reaction (ORR) is also formed on the basis of the pore-rich N-doped graphene structure.

For the preparation of N-doped, ultralight 3D GF, a low concentration (0.35–0.4 mg mL^{-1}) of homogeneous graphene oxide (GO) aqueous suspension mixed with 5 vol% pyrrole was hydrothermally treated in a Teflon-lined autoclave at 180°C for 12 h to form a N-containing gel, which was then freeze-dried and annealed at 1050°C for 3 h under Ar atmosphere. Because of the conjugated structure of pyrrole with its electron-rich N atom, it can attach to the surfaces and galleries of GO sheets through hydrogen-bonding or π–π interactions, thus providing an N source (Figure S1). The pyrrole also works as swelling agent to effectively prevent GO from self-stacking during the hydrothermal process, thus leading to the formation of the large volume GF (Figure S2). A low concentration (e.g., 0.35 mg mL^{-1}) of GO dispersion with pyrrole allows the assembly of 3D porous graphene networks (Figure 1a); this does not occur in the absence of pyrrole (Figure S3). Production of lager amounts of GF is possible by scale up of the autoclave (Figure S4).

The as-prepared GF has an ultralow density of 2.1 ± 0.3 mg cm^{-3}, which is comparable to that of the lightest silica aerogels (2–3 mg cm^{-3}),[11] close to that of CNT sheets (1.5 mg cm^{-3}),[12] and is the lowest density achieved to date among all the reported 3D graphene structures (Table S1). The ultralight weight allows a 2.4 cm^3 GF sample standing stably on the top of a dandelion, without deforming the dandelion at all (Figure 1b). Despite the ultralow density, GF has a high conductivity of 1.2 ± 0.2 × 10^3 S m^{-1}, comparable to that of graphene fiber.[13]

The ultralow density is directly ascribed to the rich open-pore structures interpenetrating the graphene skeleton (Figure 1c). The Brunauer–Emmett–Teller (BET) nitrogen adsorption isotherm reveals a specific surface area of approximately 280 m^2 g^{-1} (Figure S5), which is slightly higher than that of monolithic graphene aerogels,[14] suggesting the predominant macroporous structure of ultralight GF[15] in consistence with SEM observation (Figure 1c). The walls of GF are almost transparent under the SEM electron irradiation (Figure 1d), and extensive TEM investigations show that the thin walls typically consist of only few layers of graphene sheets (Figure 1e). The X-ray diffraction (Figure S6) and electron diffraction patterns (Figure 1f) further

[*] Y. Zhao, C. Hu, Y. Hu, H. Cheng, Prof. L. Qu
Key Laboratory of Cluster Science, Ministry of Education
School of Chemistry, Beijing Institute of Technology
Beijing 100081 (China)
E-mail: lqu@bit.edu.cn
Prof. G. Shi
Department of Chemistry, Tsinghua University
Beijing 100084 (China)
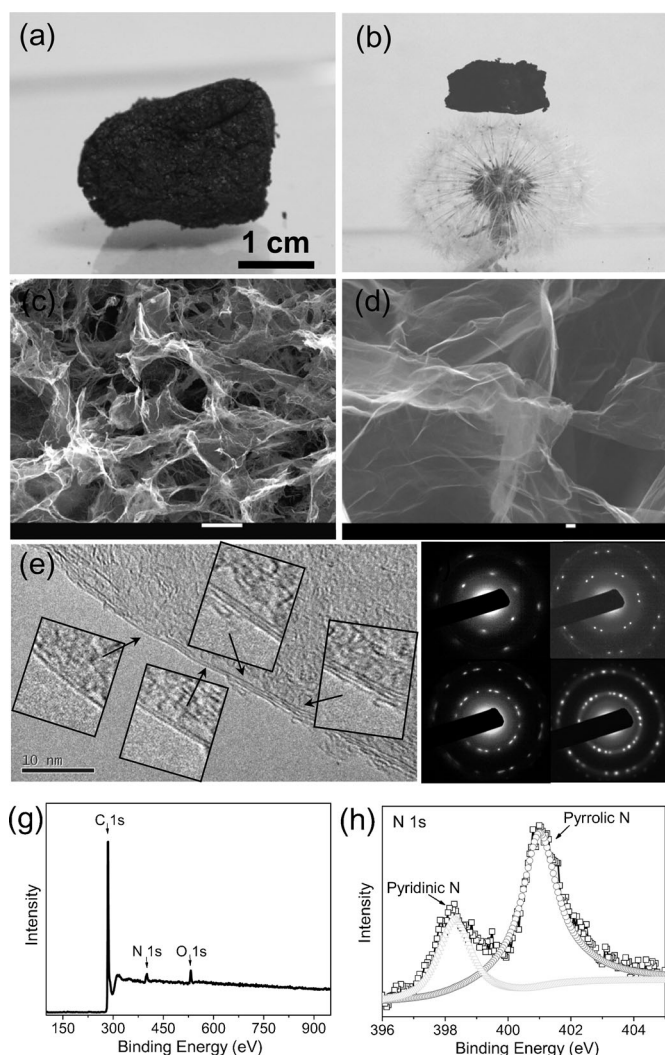
Figure 1. a,b) Photographs of an as-prepared superlight GF and one with a piece of GF size of 1.8 cm × 1.1 cm × 1.2 cm standing on a dandelion. c,d) SEM images of the sample in (a). e,f) Typical TEM images of the walls of GF and the corresponding electron diffraction patterns consistent with 1–4 crystalline graphene layers. g,h) XPS spectrum of superlight GF and the corresponding high-resolution N1s peak. Scale bars: c) 10 μm, d) 100 nm, e) 10 nm.

support the production of high-quality graphene sheets and confirm a layer number of 1–4 as demonstrated by the multiple overlaps of diffraction spots related to individual crystalline graphene sheet.

X-ray photoelectron spectroscopy (XPS) shows GF has a predominant graphitic C1s peak at around 284.8 eV, a weak O1s peak at around 532 eV, and a pronounced N1s peak located at around 400 eV without evidence of impurities (Figure 1 g), which verifies the doping of N atoms within GF (4.2% N/C atomic ratio). Consistently, elemental analysis presented a N/C atomic ratio of 4.9%. Similar to N-doped graphene sheets prepared by CVD,[9a] the high-resolution N1s spectrum of GF reveals the presence of both pyridine-like (398.5 eV) and pyrrolic (401 eV) N atoms (Figure 1 h), suggesting N atoms have been incorporated into the carbon–carbon bonds of graphenes.

In spite of the ultralow density, GF has an excellent thermal stability. When repeatedly burned on a hot flame under ambient atmosphere (Figure 2 a and Movie S1), the inherent 3D porous structure of GF remains intact (Figure 2 b). Thermogravimetric analysis (TGA) verifies the as-prepared GF has a weight loss of less than 10% at a temperature of up to 1200 °C in N_2 and it can tolerate a high temperature of approximately 600 °C in the air (Figure 2 c). Furthermore, the GF can undergo relatively large deformations (e.g., 60%) under manual compression and recover most of its material volume elastically (Figure S7). This property is attributed to the 3D self-supported structure of the high-quality graphene sheets in GF.

The highly porous and mechanically stable graphene skeleton of GF provides an ideal platform for high-efficiency adsorption that is crucial for separation/extraction of specific substances, such as oils or other organic pollutants. Figure 2 d shows the evolvement of adsorbing the gasoline dyed with Sudan III. 300 mg gasoline was adsorbed by a 1.2 mg GF block without any pretreatment within 6 seconds (Movie S2), showing an average adsorption rate of 41.7 g per gram of GF per second. The efficiency of adsorption can be referred to as weight gain, that is, wt%, defined as the weight of adsorbed substances per unit weight of pristine GF. The adsorption capacity for gasoline can be as high as about 2.77×10^2 g g^{-1} (Figure 2 e). Importantly, the adsorbed oil or solvents could be removed from the thermally-stable GF sorbent by direct combustion in air for recycled use (Figure S8).

The GF exhibits an excellent adsorption capacity for various classes of organic liquids including common daily pollutants and organic solvents (Figure 2 e). In particular, GF can adsorb amounts of the liquids up to 200 to 600 times its own weight, which is much higher than other typical carbonaceous sorbents (Table S2 and Figure 2 f) such as graphene foam (10–37 times),[10a] sponge (20–86 times),[4a] aerogel (13–27 times),[4e] carbon nanofiber aerogels (40–115 times),[10c] and CNT sponge (80–180 times).[10b] These results demonstrate the great promise of GF as a new super adsorption materials for high-efficiency recyclable sorbent applications.

Graphenes have been regarded as one attractive candidate for ultracapacitor electrode materials due to their large surface areas and high conductivities.[2, 16] However, pure graphene-based electrodes can only reach an EDL capacitance of less than 200 F g^{-1} in either aqueous or organic electrolytes as a result of the strong stack of graphene sheets,[17] Our GF provides a novel electrode material advantageously combining the unique 3D porous structure of few-layer graphenes which maximizes the exposure of their surfaces to electrolyte with effective N-doping to further enhance the capacitance performance.[18]

As expected, GF electrodes in both two-electrode (Figure S9, S10) and three-electrode (Figure 3) system presented high-performance capacitive behaviors. Figure 3a shows cyclic voltammogram (CV) curves of GF electrode in a three-electrode system with different scan rates, the curves exhibit an approximately rectangular shape, characteristic of the ideal double-layer capacitor. Accordingly, the galvanostatic charge–discharge curves at different current densities in Figure 3b exhibit a symmetric triangle feature
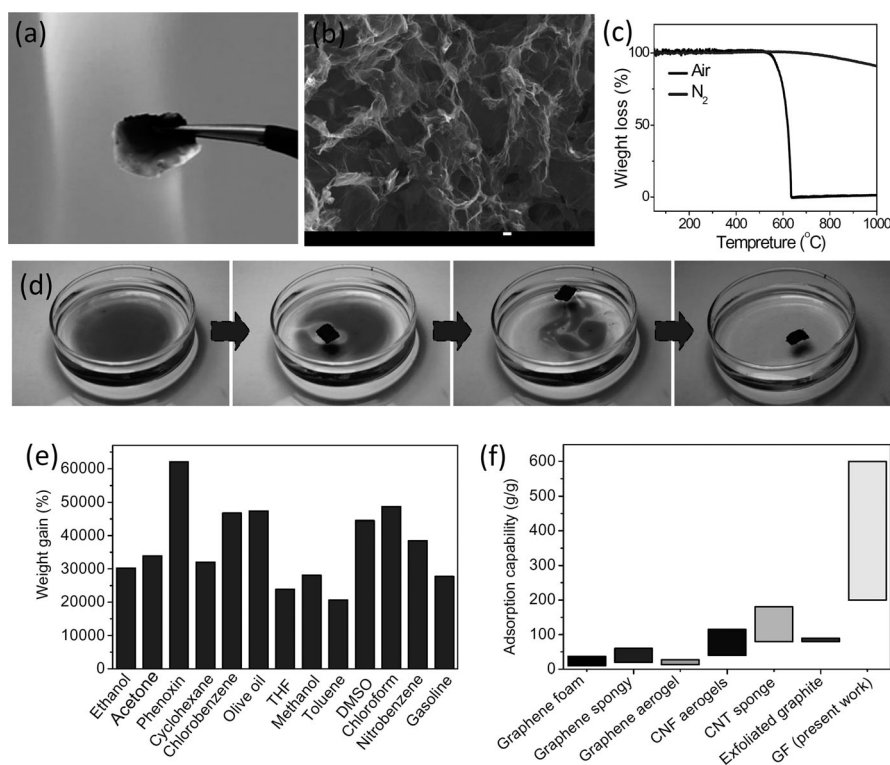
Figure 2. a) A photograph of GF in a hot flame (see Movie S1). b) SEM image of the burned GF. Scale bar is 1 μm. c) TGA curves of GF in N_2 (upper trace) and air (lower trace). d) GF adsorbing gasoline dyed with Sudan III (see Movie S2). e) Adsorption efficiency of GF in terms of weight gain. f) The comparison of adsorption capacities of different carbon-based materials (Table S2).
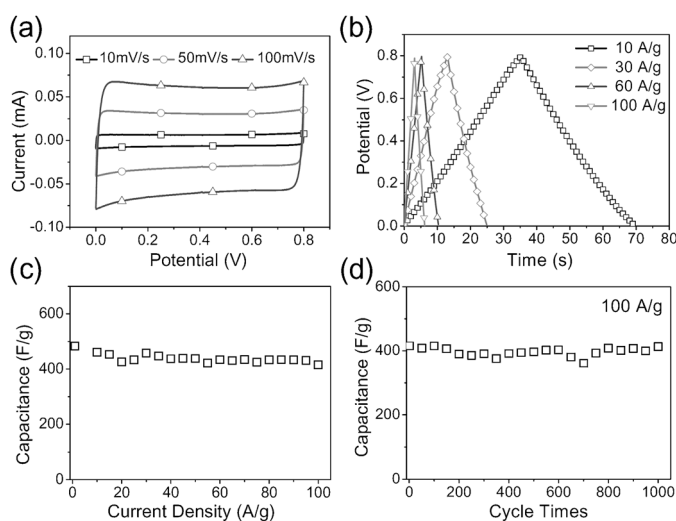

Figure 3. a) CVs of a GF electrode in 1 M $LiClO_4$ aqueous solution. b) The galvanostatic charge–discharge curves at a current density of 10, 30, 60, and 100 $A g^{-1}$. c) The specific capacitances calculated from the discharge curves under different current density. d) Cyclic stability of the GF-based capacitor with a current density of 100 $A g^{-1}$.

without obvious potential drop (IR drop).[19] At a current density of 1 $A g^{-1}$, GF presents a specific capacitance of 484 $F g^{-1}$ (Figure 3c), which is approaching to the theoretical EDL capacitance of 550 $F g^{-1}$ for pure graphene,[16a,20] and to our knowledge, is almost the highest value achieved for

graphene electrodes (Table S3).[19] Notably, the capacitor based on the GF electrode maintains a high specific capacitances at a wide range of current densities (Figure 3c) and for a long-term charge–discharge period (Figure 3d). Even at the high current density of 100 $A g^{-1}$, the capacitance still reaches 415 $F g^{-1}$, which is about 150% that of N-doped graphene film (280 $F g^{-1}$),[18c] and far above that of B and N codoped 3D graphene (under 240 $F g^{-1}$).[14] The higher capacitance of GF compared to that of 3D pure graphene (ca. 200 $F g^{-1}$),[2,10a,15] CNTs (ca. 300 $F g^{-1}$),[21] and activated carbon (ca. 300 $F g^{-1}$)[22] based electrodes could be ascribed to the highly exposed graphene sheets with minimum stack and the possible pseudo-capacitance contribution of heteroatom doping.[14,18c] These results show that GF has unique advantages as a new type of electrode material or supporting material for high performance supercapacitors.

Apart from the performance of ultralight GF in adsorption and capacitance demonstrated above, the GF can also act as efficient metal-free catalyst for oxygen reduction reaction (ORR),[9a,23] a crucial reaction happening on the cathode to enable the fuel cell work. Different from the conventional 2D stacked graphene film, GF provide a unique 3D pore-rich structure with maximum access to the N sites within highly exposed graphene sheets and multidimensional electron transport pathways. As shown in Figure 4a, a well-defined cathodic peak clearly occurred in the O_2-saturated but not N_2-saturated KOH solution for GF, in spite of the relatively large capacitive background. The linear-sweep voltammetric (LSV) measurements on a rotating disk electrode (RDE) show a one-step process, suggesting a four-electron pathway for ORR as the case for Pt/C catalyst (Figure 4b). Similar to other N-containing carbon materials for ORR,[9,24] the onset potential of ORR on GF (ca. −0.18 V) is slightly lower than that of Pt/C electrode. However, its diffusion current density is notably higher than that of Pt/C electrode over a large potential range (−0.4–−0.8 V). LSV curves at various rotation rates and Koutecky–Levich plots with a good linear relationship for the GF electrode is shown in Figure 4c and inset. The mean transferred electron number (n) per O_2 molecule involved in ORR is determined from the Koutecky–Levich equation [Eq. (S1)] to be approximately 3.7, which is similar to that calculated from the rotating ring–disk electrode (RRDE) curve [Figure 4d and Eq. (S3)], indicating the ORR proceeds via a nearly four-electron pathway.[9,24] In addition, the peroxide yield on GF is less than 20% in all the potential range and decreases to 13% at −0.8 V (Figure 4e). These
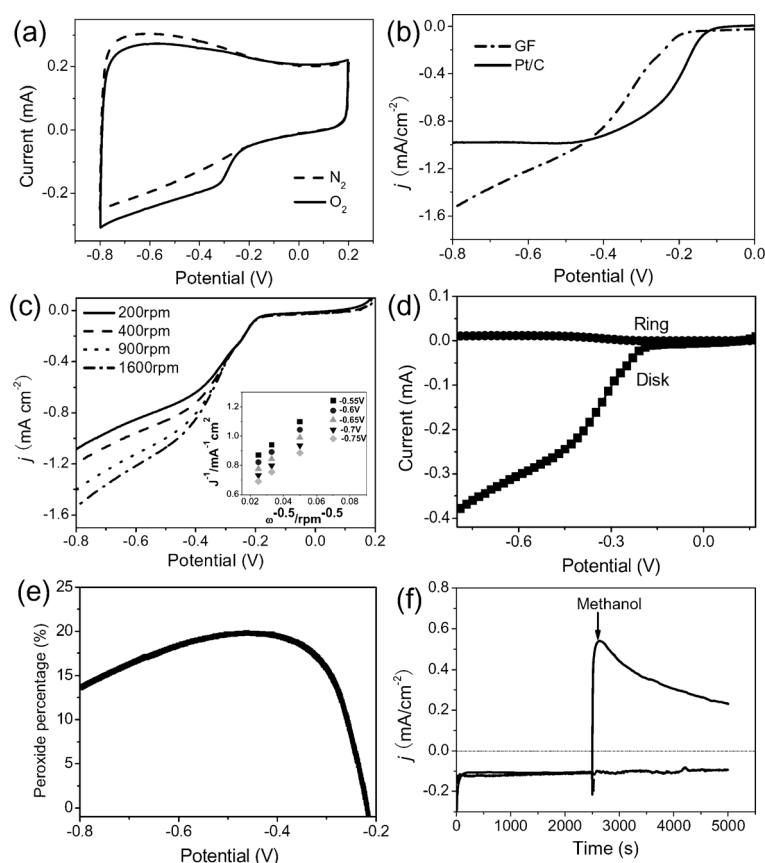
Figure 4. a) CV curves of GF in N_2-saturated and O_2-saturated 0.1 M KOH solution at a scan rate of 50 mVs^{-1}. b) LSV curves of GF (ca. 3 µg load) and Pt/C (ca. 3.3 µg load) in O_2-saturated 0.1 M KOH solution at 1600 rpm. Scan rate: 5 mVs^{-1}. c) RDE curves of GF in O_2-saturated 0.1 M KOH solution at different rotating speeds at a scan rate of 5 mVs^{-1}. Inset shows the Koutecky–Levich plots derived from RDE curves. d) RRDE curve of GF at 1600 rpm. e) The curve of peroxide yield on the GF electrode. f) Current density (j) vs time chronoamperometric responses obtained at the Pt/C (top curve) and GF (bottom curve) electrodes at −0.3 V in O_2-saturated 0.1 M KOH. The arrow indicates the addition of 10 vol% methanol into the O_2-saturated electrochemical cell.

results indicate that the N-containing GF electrode is an indeed promising metal-free catalyst for the ORR in an alkaline solution.

We also measured the electrocatalytic selectivity of the GF electrode against the electro-oxidation of the fuel molecule methanol (Figure 4 f). Remarkably, the original cathodic ORR current of the GF electrode under −0.3 V did not show an obvious change after addition of methanol (10 vol%) into the electrolyte, while a reversed anodic current was observed on Pt/C electrode associated with methanol oxidation, suggesting the excellent tolerance of the GF electrode to the crossover effect. Two days of continuous cycling in O_2-saturated 0.1 M KOH solutions demonstrates the good catalytic stability of GF electrode for ORR (Figure S11).

In summary, we have demonstrated a versatile, ultralight, N-doped, 3D graphene framework, which mainly consists of the network of only few graphene layers, and has an ultra-low density of 2.1 ± 0.3 mg cm^{-3}. Its adsorption capacity is as high as 200–600 times its own weight for common pollution and

organic solvents, much higher than that of the best carbonaceous sorbents reported previously. Based on the synergetic function of 3D open-pore structure and N doping, the GF supercapacitor has generated a high specific capacitance of 484 F g^{-1}, far superior to the typical carbon-based electrodes. Besides the potential as a new metal-free catalyst for efficient electrocatalytic ORR demonstrated in this study, the ultralight GF also provide an important platform for developing a variety of advanced devices, such as sensors and batteries.

[1] N. Hüsing, U. Schubert, *Angew. Chem.* **1998**, *110*, 22–47; *Angew. Chem. Int. Ed.* **1998**, *37*, 22–45.

[2] Y. Xu, K. X. Sheng, C. Li, G. Shi, *ACS Nano* **2010**, *4*, 4324–4330.

[3] a) S. H. Lee, H. W. Kim, J. O. Hwang, W. J. Lee, J. Kwon, C. W. Bielawski, R. S. Ruoff, S. O. Kim, *Angew. Chem.* **2010**, *122*, 10282–10286; *Angew. Chem. Int. Ed.* **2010**, *49*, 10084–10088; b) W. Chen, S. Li, C. Chen, L. Yan, *Adv. Mater.* **2011**, *23*, 5679–5683; c) Z. Tang, S. Shen, J. Zhuang, X. Wang, *Angew. Chem.* **2010**, *122*, 4707–4711; *Angew. Chem. Int. Ed.* **2010**, *49*, 4603–4607.

[4] a) H. C. Bi, X. Xie, K. B. Yin, Y. L. Zhou, S. Wan, L. B. He, F. Xu, F. Banhart, L. T. Sun, R. S. Ruoff, *Adv. Funct. Mater.* **2012**, DOI: 10.1002/adfm.201200888; b) M. A. Worsley, T. Y. Olson, J. R. I. Lee, T. M. Willey, M. H. Nielsen, S. K. Roberts, P. J. Pauzauskie, J. Biener, J. H. Satcher, Jr., T. F. Baumann, *J. Phys. Chem. Lett.* **2011**, *2*, 921–925; c) M. A. Worsley, P. J. Pauzauskie, T. Y. Olson, J. Biener, J. H. Satcher, Jr., T. F. Baumann, *J. Am. Chem. Soc.* **2010**, *132*, 14067–14069; d) Z. P. Chen, W. C. Ren, L. B. Gao, B. L. Liu, S. F. Pei, H. M. Cheng, *Nat. Mater.* **2011**, *10*, 424–428; e) H. P. Cong, X. C. Ren, P. Wang, S. H. Yu, *ACS Nano* **2012**, *6*, 2693.

[5] a) Z. S. Wu, S. B. Yang, Y. Sun, K. Parvez, X. L. Feng, K. Müllen, *J. Am. Chem. Soc.* **2012**, *134*, 9082–9085; b) C. G. Hu, H. H. Cheng, Y. Zhao, Y. Hu, Y. Liu, L. M. Dai, L. T. Qu, *Adv. Mater.* **2012**, *24*, 5493–5498.

[6] T. A. Schaedler, A. J. Jacobsen, A. Torrents, A. E. Sorensen, J. Lian, J. R. Greer, L. Valdevit, W. B. Carter, *Science* **2011**, *334*, 962–965.

[7] M. Mecklenburg, A. Schuchardt, Y. K. Mishra, S. Kaps, R. Adelung, A. Lotnyk, L. Kienle, K. Schulte, *Adv. Mater.* **2012**, *24*, 3486–3490.

[8] a) X. R. Wang, X. L. Li, L. Zhang, Y. Yoon, P. K. Weber, H. L. Wang, J. Guo, H. J. Dai, *Science* **2009**, *324*, 768–771; b) H. B. Wang, T. Maiyalagan, X. Wang, *ACS Catal.* **2012**, *2*, 781–794; c) S. Y. Wang, L. P. Zhang, Z. H. Xia, A. Roy, D. W. Chang, J. B. Baek, L. M. Dai, *Angew. Chem.* **2012**, *124*, 4285–4288; *Angew. Chem. Int. Ed.* **2012**, *51*, 4209–4212.

[9] a) L. T. Qu, Y. Liu, J. B. Baek, L. M. Dai, *ACS Nano* **2010**, *4*, 1321–1326; b) Y. Li, Y. Zhao, H. H. Cheng, Y. Hu, G. Q. Shi, L. M. Dai, L. T. Qu, *J. Am. Chem. Soc.* **2012**, *134*, 15–18.

[10] a) Z. Q. Niu, J. Chen, H. H. Hng, J. Ma, X. D. Chen, *Adv. Mater.* **2012**, *24*, 4144–4150; b) X. C. Gui, J. Q. Wei, K. L. Wang, A. Y. Cao, H. W. Zhu, Y. Jia, Q. K. Shu, D. H. Wu, *Adv. Mater.* **2010**, *22*, 617–621; c) H. W. Liang, Q. F. Guan, L. F. Chen, Z. Zhu, W. J. Zhang, S. H. Yu, *Angew. Chem. Int. Ed.* **2012**, *51*, 5101–5105.

[11] N. Leventis, C. S. Leventis, G. H. Zhang, A. M. Rawashdeh, *Nano. Lett.* **2002**, *2*, 957–960.

[12] M. Zhang, S. Fang, A. A. Zakhidov, S. B. Lee, A. E. Aliev, C. D. Williams, K. R. Atkinson, R. H. Baughman, *Science* **2005**, *309*, 1215–1219.

[13] Z. L. Dong, C. C. Jiang, H. H. Cheng, Y. Zhao, G. Q. Shi, L. Jiang, L. T. Qu, *Adv. Mater.* **2012**, *24*, 1856–1861.

[14] Z. S. Wu, A. Winter, L. Chen, Y. Sun, A. Turchanin, X. L. Feng, K. Müllen, *Adv. Mater.* **2012**, *24*, 5130–5135.

[15] L. Zhang, G. Q. Shi, *J. Phys. Chem. C* **2011**, *115*, 17206–17212.

[16] a) M. D. Stoller, S. J. Park, Y. W. Zhu, J. H. An, R. S. Ruoff, *Nano Lett.* **2008**, *8*, 3498–3502; b) Y. Wang, Z. Shi, Y. Huang, Y. Ma, C. Wang, M. Chen, Y. Chen, *J. Phys. Chem. C* **2009**, *113*, 13103–13107; c) D. W. Wang, F. Li, Z. S. Wu, W. Ren, H. M. Cheng, *Electrochem. Commun.* **2009**, *11*, 1729–1732.

[17] a) T. Y. Kim, H. W. Lee, M. Stoller, D. R. Dreyer, C. W. Bielawski, R. S. Ruoff, K. S. Suh, *ACS Nano* **2011**, *5*, 436–442;

b) Y. Zhu, S. Murali, W. Cai, X. Li, J. W. Suk, J. R. Potts, R. J, R. S. Ruoff, *Adv. Mater.* **2010**, *22*, 3906–3924.

[18] a) Y. C. Qiu, X. F. Zhang, S. H. Yang, *Phys. Chem. Chem. Phys.* **2011**, *13*, 12554–12558; b) H. M. Jeong, J. W. Lee, W. H. Shin, Y. J. Choi, H. J. Shin, J. K. Kang, J. W. Choi, *Nano Lett.* **2011**, *11*, 2472–2477; c) L. Sun, L. Wang, C. G. Tian, T. X. Tan, Y. Xie, K. Y. Shi, M. T. Li, H. G. Fu, *RSC Adv.* **2012**, *2*, 4498–4506.

[19] Y. Q. Sun, Q. Wu, G. Q. Shi, *Energy Environ. Sci.* **2011**, *4*, 1113–1132.

[20] J. Xia, F. Chen, J. Li, N. Tao, *Nat. Nanotechnol.* **2009**, *4*, 505–509.

[21] Y. Zhai, Y. Dou, D. Zhao, P. F. Fulvio, R. T. Mayes, S. Dai, *Adv. Mater.* **2011**, *23*, 4828–4850.

[22] L. L. Zhang, X. S. Zhao, *Chem. Soc. Rev.* **2009**, *38*, 2520–2531.

[23] a) K. P. Gong, F. Du, Z. H. Xia, M. Durstock, L. M. Dai, *Science* **2009**, *323*, 760–764; b) Y. Y. Shao, S. Zhang, M. H. Engelhard, G. S. Li, G. C. Shao, Y. Wang, J. Liu, I. A. Aksay, Y. H. Lin, *J. Mater. Chem.* **2010**, *20*, 7491–7496; c) D. S. Geng, Y. Chen, Y. G. Chen, Y. L. Li, R. Y. Li, X. L. Sun, S. Y. Ye, S. Knights, *Energy Environ. Sci.* **2011**, *4*, 760–764.

[24] a) S. Y. Wang, D. S. Yu, L. M. Dai, *J. Am. Chem. Soc.* **2011**, *133*, 5182–5185; b) Y. Zheng, Y. Jiao, J. Chen, J. Liu, J. Liang, A. J. Du, W. M. Zhang, Z. H. Zhu, S. C. Smith, M. Jaroniec, G. Q. Lu, S. Z. Qiao, *J. Am. Chem. Soc.* **2011**, *133*, 20116–20119.